Available online at www.sciencedirect.com
SCIENCE DIRECT®
Journal of Membrane Science 241 (2004) 207–218
journal of MEMBRANE SCIENCE
www.elsevier.com/locate/memsci

Hydrogen permeance of palladium–copper alloy membranes over a wide range of temperatures and pressures

B.H. Howard [a,*], R.P. Killmeyer [a], K.S. Rothenberger [a], A.V. Cugini [a], B.D. Morreale [b], R.M. Enick [c], F. Bustamante [c]

[a] *United States Department of Energy, National Energy Technology Laboratory (NETL), P.O. Box 10940, Pittsburgh, PA 15236, USA*
[b] *NETL Site Support Contractor, Parsons Project Services Inc., P.O. Box 618, South Park, PA 15129, USA*
[c] *NETL Research Associate, University of Pittsburgh, Department of Chemical and Petroleum Engineering, Pittsburgh, PA 15261, USA*

Received 1 August 2003; received in revised form 2 April 2004; accepted 8 April 2004

Abstract

The permeance of Pd–Cu alloys containing 40, 53, 60, and 80 wt.% Pd has been determined over the 623–1173 K temperature range for H_2 partial pressure differences as great as 2.6 MPa. Pure palladium and copper membranes were also evaluated. The Pd–Cu alloys exhibited predictable permeances that reflected the crystalline phase structures as shown in the binary phase diagram. Under conditions of face-centered-cubic (fcc) stability, the permeance increased steadily with palladium content, approaching the permeance of pure palladium membranes. The 53 and 60 wt.% Pd alloys were evaluated at temperatures within the body-centered-cubic (bcc) stability region. For both alloys, the bcc permeance was several times greater than the fcc permeance with the 60 wt.% Pd bcc permeance at 623 K reaching about 70% of the permeance of palladium. These bcc alloys were subjected to temperature increases during testing that resulted in transition from bcc to fcc, followed by temperature decreases that should revert the alloys to bcc. The permeances dropped abruptly during the transition from bcc to fcc. However, on cooling back to the bcc stability region, neither the 60 nor 53 wt.% Pd alloy completely regained a bcc permeance during the test period. All of the Pd–Cu alloys subjected to testing at 1173 K showed some permeance decline that was attributed to intermetallic diffusion between the membrane and support. The application of a diffusion barrier between the support and membrane foil in a 53 wt.% Pd permeance test successfully blocked the intermetallic diffusion and prevented degredation of the membrane's performance.

Keywords: Gas separations; Inorganic membranes; Metal membranes; Hydrogen; Palladium–copper

1. Introduction

Hydrogen production is expected to increase in the future as the US moves toward widespread use of hydrogen as an energy carrier. Industrial processes, such as coal gasification, can be used for the production of hydrogen from domestic energy sources; however, hydrogen produced in this way is mixed with carbon dioxide and other gases requiring ancillary separation processes impacting the cost of hydrogen production. Advances in membrane technology have the potential to improve the efficiency of hydrogen separation and recovery and reduce the cost associated with hydrogen production.

Membrane poisoning by the contaminants typically found in gasifier effluent streams has been identified as a substantial scientific hurdle impeding the implementation of membrane technology in the generation of hydrogen via gasification. These contaminants include S, Cl and Hg compounds which are known poisons to palladium-based membranes [1–4]. Sulfur in the form of H_2S is of special interest in the gasification of coal and other fossil fuels. Thus, the development of a robust, poison resistant and economical hydrogen membrane material is necessary for successful implementation of advanced fossil energy plants. Recent studies have reported that palladium–copper alloy materials possess the high permeability [5–12] and resistance to sulfur poisoning needed to be considered as viable candidates for hydrogen separation within the coal gasification scheme [5,6,13,14].

The highest reported values of Pd–Cu alloy permeability were comparable to the permeability of pure palladium

* Corresponding author. Tel.: +412 386 5908; fax: +412 386 5920.
E-mail address: bret.howard@netl.doe.gov (B.H. Howard).

0376-7388/$ – see front matter © 2004 Elsevier B.V. All rights reserved.
doi:10.1016/j.memsci.2004.04.031

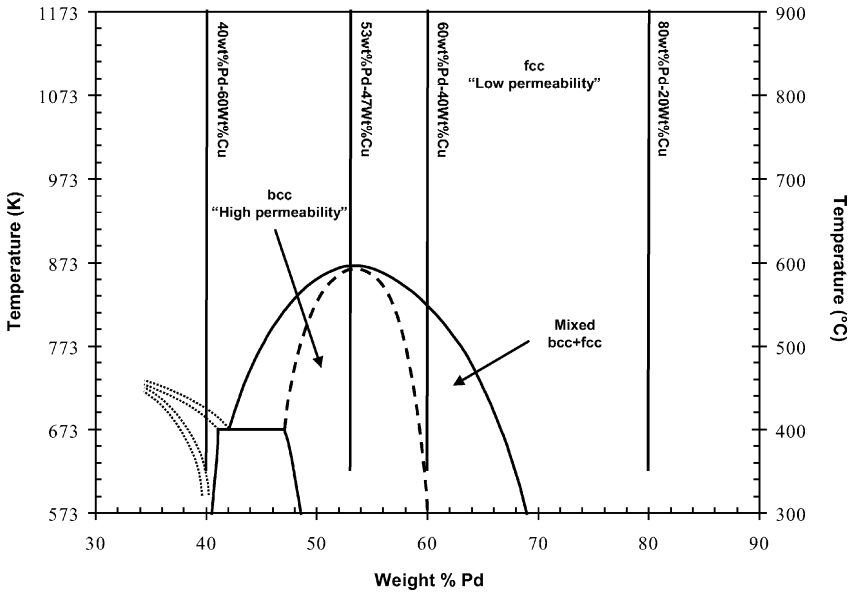

Fig. 1. Pd–Cu phase diagram based on data summarized by Subramanian and Laughlin [18] and Henson [19]. Vertical lines represent alloy compositions and temperature ranges examined in this study.

and occurred for a composition of 60 wt.% Pd–40 wt.% Cu [5,7,9,15]. High permeability values at this particular composition are attributed to the high mobility of hydrogen atoms within the body-centered-cubic (bcc) crystal structure of the Pd–Cu alloy [15–19] relative to the face-centered-cubic (fcc) continuous solid solution. Fig. 1 shows the fcc, bcc and mixed phase regions in the portion of the Pd–Cu binary phase diagram of interest in this study. Dissolved hydrogen is known to shift the stability range of the bcc and mixed bcc–fcc phase regions to slightly higher palladium concentrations, however, the maximum temperature at which any bcc phase is stable remains at about 873 K [15].

Attempts to make Pd–Cu alloy membranes more economically viable have focused on the manufacture of ultra-thin Pd–Cu alloys on porous substrates. Roa and coworkers are investigating the electroless deposition of thin films (1–10 μm) of Pd–Cu alloys on porous ceramic substrates [20,21]. Ma et al. have employed electroless deposition techniques to prepare thin films of Pd–Cu alloys on porous stainless steel substrates [22].

Previous literature assessments of the permeability of Pd–Cu alloys have typically been determined at low H_2 partial pressure over a limited range of low temperatures, with most data being generated for the 60 wt.% Pd alloy (Table 1). In contrast, the objective of the current study was to assess the hydrogen permeability of Pd–Cu alloys over the wide ranges of temperature and pressure associated with conceptual, gasifier and post-gasifier, water-gas shift membrane reactors and to correlate the measured permeabilities with membrane alloy crystal structure. Four Pd–Cu alloys were selected, 40 wt.% Pd (a copper-rich composition outside of the bcc phase region), 53 wt.% Pd (the composition in the center of the bcc phase region), 60 wt.% Pd (the composition most commonly cited as yielding the greatest H_2 permeability) and 80 wt.% Pd (a composition far removed from the bcc phase region and intermediate to the 60 wt.% Pd alloy and pure palladium). The permeability values of palladium and copper membranes were also included in this evaluation. The Pd–Cu alloys in this work will be referred to by palladium content in weight percent with the balance understood to be copper.

2. Experimental

Palladium–copper alloy foils, 99.9% purity, 0.1 mm (100 μm) thick, were prepared by ACI Alloys, San Jose, CA. Palladium foil, 99.9% purity, 0.1 mm thick, and copper foil, 1.0 mm thick, were obtained from Alfa Aesar. All foil samples were cleaned prior to brazing by sanding/polishing with 800 grit silicon carbide paper to remove surface oxides. This was followed by an acetone rinse and a deionized water rinse. Membranes were fabricated for testing by brazing foil octagons to thick nickel alloy washers having negligible hydrogen permeability using high-purity gold powder as the filler metal and boric acid as a flux. Brazing was done in a muffle furnace at 1400 K. After brazing, residual flux was dissolved by soaking membranes in 363 K deionized water for a minimum of 12 h followed by several rinses. An example of a mounted membrane is shown in the inset in Fig. 2. A porous Hastelloy support was utilized on the permeate side of the membrane foil to prevent foil distortion and possible mechanical failure at high temperatures in the presence of a pressure drop. The membrane surface contacted the porous support surface but was not bonded

Table 1
Summary of reported Pd–Cu alloy permeances and permeabilities

Reference	X_M	T (K)	$1/T$ (K^{-1})	$P_{H_2,ret}$ (kPa)	$P_{H_2,perm}$ (kPa)	Permeance (mol m^{-2} s^{-1} Pa^{-n})	Permeability (mol m^{-1} s^{-1} Pa^{-n})	n	Pd:Cu (wt.% Pd)
McKinley [7]	25.4	623	0.00161	618	101.3	0	0	0.5	10
McKinley [7]	25.4	623	0.00161	2169	101.3	0	0	0.5	10
McKinley [7]	25.4	623	0.00161	618	101.3	0	0	0.5	20
McKinley [7]	25.4	623	0.00161	2169	101.3	0	0	0.5	20
McKinley [7]	25.4	623	0.00161	618	101.3	0	0	0.5	40
McKinley [7]	25.4	623	0.00161	2169	101.3	0	0	0.5	40
McKinley [7]	25.4	623	0.00161	618	101.3	2.79E−06	7.09E−11	0.5	45
McKinley [7]	25.4	623	0.00161	2169	101.3	6.78E−06	1.72E−10	0.5	45
McKinley [7]	25.4	623	0.00161	618	101.3	8.93E−05	2.27E−09	0.5	55
McKinley [7]	25.4	623	0.00161	2169	101.3	9.27E−05	2.35E−09	0.5	55
McKinley [7]	25.4	623	0.00161	618	101.3	2.61E−04	6.81E−09	0.5	58
McKinley [7]	25.4	623	0.00161	2169	101.3	2.71E−04	6.89E−09	0.5	58
Edlund and McCarthy [24]	15	673	0.00149	791	101.3	1.59E−03	2.39E−08	0.5	60
Edlund and McCarthy [24]	15	673	0.00149	791	101.3	1.30E−03	1.96E−08	0.5	60
Edlund and McCarthy [24]	17	673	0.00149	791	101.3	1.23E−03	2.08E−08	0.5	60
Edlund and McCarthy [24]	17	673	0.00149	791	101.3	1.15E−03	1.95E−08	0.5	60
Edlund and McCarthy [24]	25	673	0.00149	791	101.3	7.82E−04	1.96E−09	0.5	60
Juda et al. [11]	17	673	0.00149	239.2	101.3	8.72E−04	1.48E−08	0.5	60
McKinley [7]	25.4	423	0.00236	618	101.3	1.68E−04	4.26E−09	0.5	60
McKinley [7]	25.4	473	0.00211	618	101.3	2.04E−04	5.18E−09	0.5	60
McKinley [7]	25.4	523	0.00191	618	101.3	5.00E−04	1.27E−08	0.5	60
McKinley [7]	25.4	573	0.00175	618	101.3	6.51E−04	1.65E−08	0.5	60
McKinley [7]	25.4	623	0.00161	618	101.3	5.82E−04	1.48E−08	0.5	60
McKinley [7]	25.4	623	0.00161	2169	101.3	6.63E−04	1.96E−08	0.5	60
McKinley [7]	25.4	623	0.00161	618	101.3	5.81E−04	1.48E−08	0.5	60
McKinley [7]	25.4	623	0.00161	2169	101.3	1.41E−04	3.59E−08	0.5	60
McKinley [7]	25.4	623	0.00161	618	101.3	7.29E−04	1.85E−08	0.5	60
McKinley [7]	25.4	673	0.00149	618	101.3	8.21E−04	2.09E−08	0.5	60
McKinley [7]	25.4	723	0.00138	618	101.3	7.68E−04	1.95E−08	0.5	60
McKinley [7]	25.4	773	0.00129	618	101.3	4.44E−04	1.28E−08	0.5	60
McKinley [7]	25.4	823	0.00122	618	101.3	1.90E−04	4.82E−09	0.5	60
McKinley [5]	25.4	623	0.00161	618	101.3	5.80E−04	1.47E−08	0.5	60
Roa et al. [21]	1.5	623	0.00161		83	3.76E−03	5.63E−09	0.5	60
Roa et al. [21]	1.5	723	0.00138	273	83	1.86E−03	2.79E−09	0.5	60
McKinley [7]	25.4	623	0.00161	618	101.3	3.85E−04	9.79E−09	0.5	62.5
McKinley [7]	25.4	623	0.00161	2169	101.3	4.32E−04	1.10E−08	0.5	62.5
Nam and Lee [12]	2	623	0.00161	170.6	101.3	8.05E−06	1.61E−11	1	63
Nam and Lee [12]	2	623	0.00161	170.6	101.3	7.51E−06	1.50E−11	1	63
Nam and Lee [12]	2	623	0.00161	170.6	101.3	4.83E−06	9.65E−12	1	63
McKinley [7]	25.4	623	0.00161	618	101.3	4.19E−05	1.06E−09	0.5	70
McKinley [7]	25.4	623	0.00161	2169	101.3	1.12E−04	2.84E−09	0.5	70
Roa et al. [21]	1–25	623	0.00161		83	–	2.08E−09	0.5	70
Roa et al. [21]	1–25	623	0.00161		83	–	1.71E−09	0.5	70
Roa et al. [20]	1.5	623	0.00161	446	101.3	1.89E−03	2.83E−09	0.5	70
Roa et al. [20]	27.6	773	0.00129	790.8	101.3	8.41E−05	2.32E−09	0.5	72
Ma et al. [22]	35.2	623	0.00161	405.3	101.3	4.87E−05	1.71E−09	0.5	74
Ma et al. [22]	33.6	623	0.00161	405.3	101.3	7.40E−05	2.49E−09	0.5	78
Roa et al. [21]	12.5	723	0.00138	510	83	2.60E−04	3.25E−09	0.5	78
Roa et al. [20]	12.5	723	0.00138	446	101.3	5.15E−04	6.44E−09	0.5	78
Roa et al. [20]	11	773	0.00129	446	101.3	1.00E−03	1.10E−08	0.5	80
Roa et al. [21]	11.6	723	0.00138	510	83	3.67E−04	4.26E−09	0.5	81
Roa et al. [20]	11.6	773	0.00129	446	101.3	1.49E−03	1.73E−08	0.5	81
Grashoff et al. [8]	NA	813	0.00123	446	101.3	NA	1.18E−08	0.5	90
McKinley [7]	25.4	623	0.00161	618	101.3	2.60E−04	6.61E−09	0.5	90
McKinley [7]	25.4	623	0.00161	2169	101.3	2.78E−04	7.06E−09	0.5	90
McKinley [7]	25.4	623	0.00161	618	101.3	2.60E−04	6.60E−09	0.5	90
McKinley [7]	25.4	623	0.00161	2169	101.3	2.78E−04	7.06E−09	0.5	90
McKinley [5]	25.4	623	0.00161	618	101.3	2.59E−04	6.58E−09	0.5	90
Roa et al. [21]	1	623	0.00161	510	83	8.42E−04	8.42E−10	0.5	90
Roa et al. [21]	12	723	0.00138	510	83	6.27E−04	7.53E−09	0.5	91
Roa et al. [21]	1–25	623	0.00161		83	-	7.34E−10	0.5	91
Roa et al. [20]	12	773	0.00129	446	101.3	2.29E−03	2.75E−08	0.5	91

Table 1 (*Continued*)

Reference	X_M	T (K)	$1/T$ (K^{-1})	$P_{H_2,ret}$ (kPa)	$P_{H_2,perm}$ (kPa)	Permeance (mol m^{-2} s^{-1} Pa^{-n})	Permeability (mol m^{-1} s^{-1} Pa^{-n})	n	Pd:Cu (wt.% Pd)
Roa et al. [21]	1–25	623	0.00161		83	–	9.78E−10	0.5	93
Uemiya et al. [10]	18.9	473	0.00211	303.9	101.3	4.31E−05	8.14E−10	0.5	93.8
Uemiya et al. [10]	18.9	523	0.00191	303.9	101.3	7.11E−05	1.34E−09	0.5	93.8
Uemiya et al. [10]	18.9	573	0.00175	303.9	101.3	1.06E−04	2.00E−09	0.5	93.8
Uemiya et al. [10]	18.9	623	0.00161	303.9	101.3	1.43E−04	2.71E−09	0.5	93.8
Uemiya et al. [10]	18.9	673	0.00149	303.9	101.3	1.93E−04	3.65E−09	0.5	93.8
Uemiya et al. [10]	18.9	723	0.00138	303.9	101.3	2.36E−04	4.46E−09	0.5	93.8
Uemiya et al. [10]	18.9	773	0.00129	303.9	101.3	3.52E−04	6.65E−09	0.5	93.8
Grashoff et al. [8]	NA	813	0.00123	446	101.3	NA	1.60E−08	0.5	95
Grashoff et al. [8]	NA	813	0.00123	446	101.3	NA	1.98E−08	0.5	100
McKinley [7]	25.4	623	0.00161	618	101.3	3.97E−04	1.01E−08	0.5	100
McKinley [7]	25.4	623	0.00161	2169	101.3	4.89E−04	1.24E−08	0.5	100

to it. The assembly was TIG welded under argon with care taken to minimize the membrane temperature during the procedure. The resulting mounted membranes, shown in an exploded view in Fig. 2, had an active hydrogen permeation diameter of 8.5 mm. The membrane brazing and mounting techniques were developed at the US Department of Energy (DOE)'s National Energy Technology Laboratory (NETL).

The copper membrane was prepared by a different technique due to the incompatibility of the brazing procedure with the low melting point of copper. A 19.1 mm diameter disk was punched from the 1.0 mm thick copper sheet and cleaned as described earlier. This disk was TIG welded under argon between two Inconel® 600 tubes. No porous support was used. Alloying of the Inconel® tubing with the copper membrane edge at the welded joint prevented potential loss of hydrogen from the reactor via this route.

Some membranes were annealed for crystal structure control following mounting. Annealing was carried out by placing the mounted membrane in a tube furnace at a selected temperature under flowing nitrogen. The membrane was held at temperature for a set period of time, quenched and characterized by X-ray diffraction (XRD) to verify structure.

A diffusion barrier was employed in some experiments to prevent intermetallic diffusion from occurring between the membrane foils and porous support. This was especially necessary at the upper extreme of the temperature range of this study. The diffusion barrier consisted of a layer of porous anodic alumina having a pore size of about 0.2 μm and a thickness of about 100 μm that was sandwiched between the membrane foil and support.

The hydrogen membrane testing (HMT) unit used in this study was designed and constructed at NETL and has been described previously [23]. The apparatus was designed to allow testing of hydrogen membranes at pressures and temperatures up to 3.1 MPa and 1173 K, respectively. A simplified schematic of the HMT unit is illustrated in Fig. 3. The membrane assembly consisted of two 9.5 mm o.d. Inconel® 600 tubes placed concentrically inside the 19.1 mm o.d. Inconel®

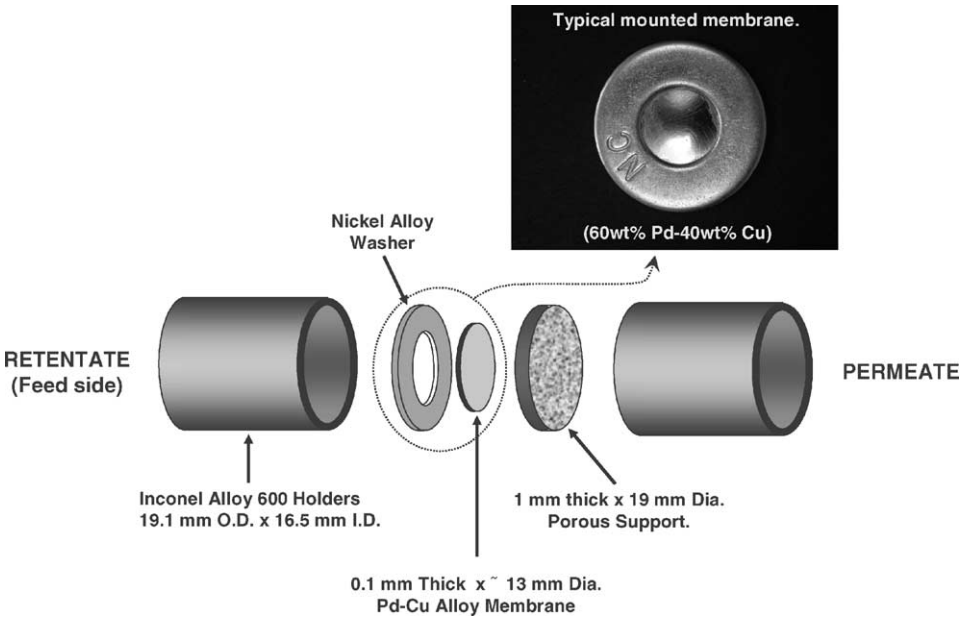

Fig. 2. Schematic of the palladium–copper alloy membrane assembly.

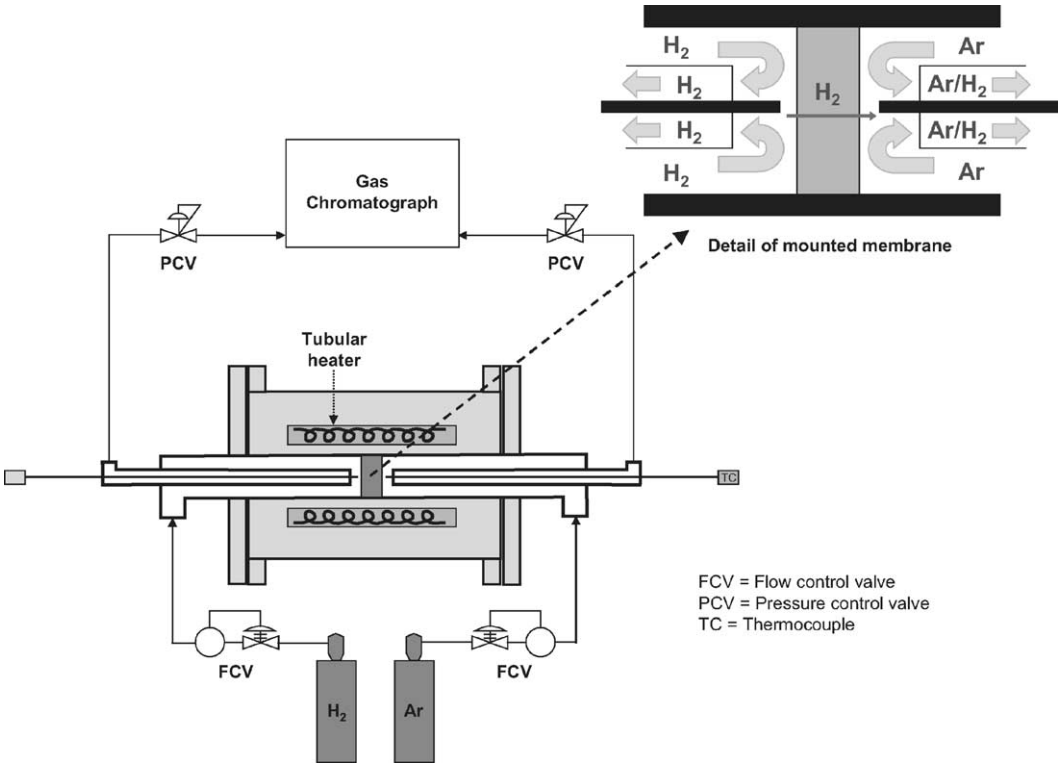

Fig. 3. Schematic of membrane testing apparatus used for this study.

600 extension tubes approximately 6 mm from the membrane surface, as shown in Fig. 2. This coaxial tube configuration allowed the feed and sweep gases to enter through the annulus between the 19.1 and 9.5 mm o.d. tubes, contact the membrane, and exit through the inside of the 9.5 mm o.d. tube. The membrane unit was heated by a 152-mm long cylindrical resistance heater placed concentrically around the membrane assembly. Temperatures were measured using type-K thermocouples placed approximately 4 mm from each side of the membrane surface. The membrane unit and resistance heater were insulated with ceramic fiber insulation and housed inside an 8 liter stainless steel purge vessel that was continuously flushed with nitrogen. The purge vessel was used to ensure that any fugitive hydrogen evolved from the unit would be diluted, cooled, and vented safely.

The membrane unit feed gas consisted of a mixture of 90% hydrogen and 10% helium while ultra-high-purity argon was used for the permeate sweep gas. For this study, the sweep gas pressure was controlled to maintain a small total pressure gradient of 0.14 MPa, although the hydrogen partial pressure drop was as high as 2.6 MPa. Flow rates were controlled by Brooks mass flow controllers, with the feed flow ranging from 190 to 250 sccm and the sweep gas flow controlled so as to maintain the concentration of hydrogen in the permeate at generally less than 4 mol%. Water, hydrocarbon and oxygen traps were used in the gas inlet lines. The feed gas pressure was regulated by a pneumatically actuated, stainless steel control valve. The hydrogen permeating through the membrane was carried to a Hewlett-Packard 5890 Series II gas chromatograph equipped with a 3-m long by 3.2 mm o.d. zeolite-packed column and thermal conductivity detector. The detection of helium in the permeate gas was indicative of a membrane leak and resulted in termination of the test. Flows, pressures and temperatures were controlled with a PC-based process control system.

Membranes were characterized prior to and following permeance testing. Membranes were recovered following testing by cutting them out of the extension tubes using a dry-cutting power saw, making the cuts a distance from the membrane itself. The remaining extension tubing was removed by carefully cutting by hand. To allow characterization of the permeate surface of the used membranes, the support was removed by carefully hand-cutting the welded seam. Care was taken to minimize contamination in all cutting procedures. The membrane surfaces were photographed and examined through a stereomicroscope. Characterization techniques included X-ray diffraction and scanning electron microscopy (backscattered mode) with energy dispersive spectroscopy (SEM/EDS).

3. Results and discussion

The flux of hydrogen through a dense membrane is proportional to the difference of the square root of the

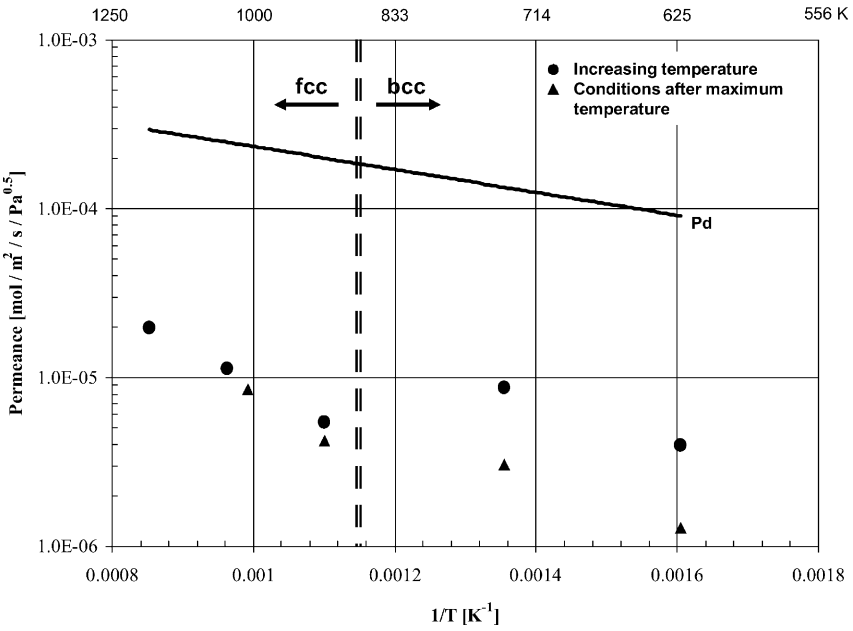

Fig. 4. Permeance of the 53 wt.% Pd alloy as a function of inverse temperature.

hydrogen partial pressures on the retentate and permeate sides of the membrane. Eqs. (1) and (2) are used to represent the performance of the membrane in terms of permeability, k (mol $H_2\,m^{-1}\,s^{-1}\,Pa^{-0.5}$), and permeance, k' (mol $H_2\,m^{-2}\,s^{-1}\,Pa^{-0.5}$), respectively.

$$N_{H_2} = k\frac{P_{H_2,ret}^{0.5} - P_{H_2,perm}^{0.5}}{X_M} \quad (1)$$

$$N_{H_2} = k'(P_{H_2,ret}^{0.5} - P_{H_2,perm}^{0.5}) \quad (2)$$

In both expressions, N_{H_2} (mol $H_2\,m^{-2}\,s^{-1}$) represents the flux of hydrogen, $P_{H_2,perm}$ (Pa) represents the hydrogen partial pressure in the permeate, and $P_{H_2,ret}$ (Pa) represents the hydrogen partial pressure in the retentate. In Eq. (1), X_M (m) is the membrane thickness. The effect of temperature on permeance was evaluated for the 53 and 60 wt.% Pd membranes. The permeance results as a function of inverse temperature are presented in Figs. 4 and 5, respectively. The permeance results for both 40 and 80 wt.% Pd membranes are presented in Fig. 6. Note that the Pd–Cu alloys are completely

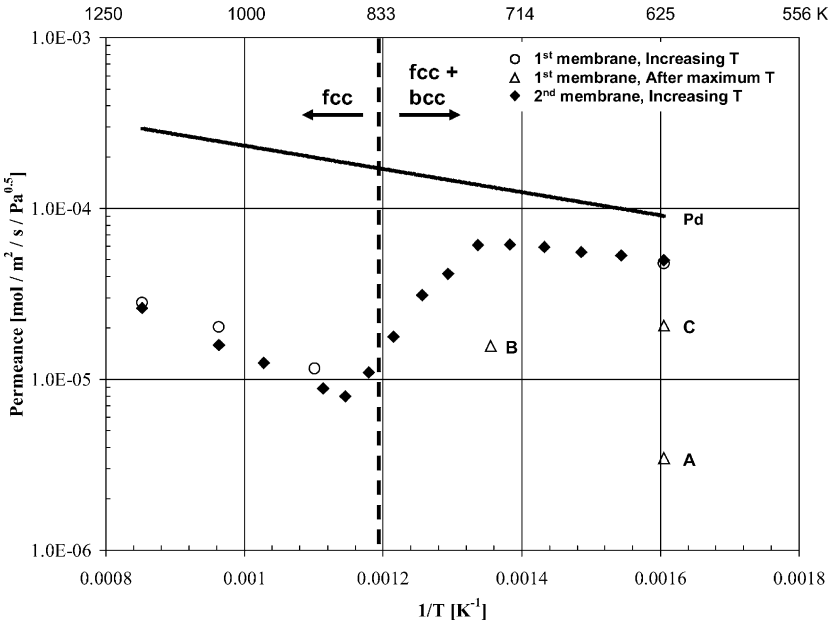

Fig. 5. Permeance of the 60 wt.% Pd alloy as a function of inverse temperature.

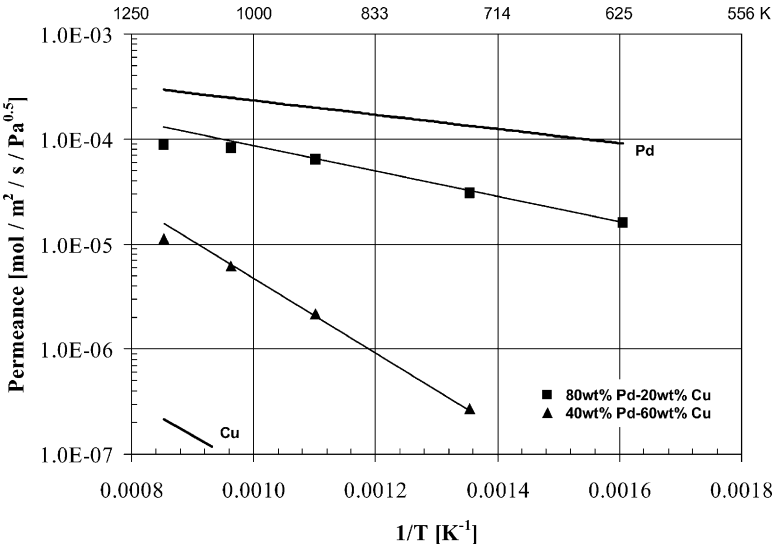

Fig. 6. Permeance of the 40 and 80 wt.% Pd alloys as a function of temperature.

selective for hydrogen. The permeance values for pure palladium membranes are included in Figs. 4–6 for comparison. The permeance of a pure copper membrane is shown in Fig. 6 for comparison to the permeance of the lowest palladium content alloy.

Table 2 summarizes the alloy phase structure determined by XRD at ambient temperature and the structure expected based on the binary phase diagram [18,19]. The 60 wt.% Pd brazed membranes were found to be fcc or mixed bcc–fcc while all other compositions had the expected low temperature structure based on the phase diagram. The quenching effect of the brazing procedure probably prevented the 60 wt.% Pd alloy from reaching low temperature equilibrium. To verify that the brazed 60 wt.% Pd alloy would convert to the expected bcc structure when flux tested, a brazed membrane was annealed at 588 K for 66 h. XRD showed that the alloy did fully convert to the bcc structure.

The 53 wt.% Pd alloy permeance was initially measured at 623 K and then at 738 K (Fig. 4). This alloy composition corresponds to the center of the bcc phase region shown in Fig. 1, which has a bcc to fcc transition temperature of 871 K and only a very narrow temperature range of mixed bcc–fcc structure. It is likely that these permeance values corresponded to the bcc structure. The values were more than an order-of-magnitude less than that of pure palladium. XRD results (Table 2) verified that this membrane was bcc as loaded into the reactor. When the membrane was heated beyond 871–908 K, the permeance diminished due to the temperature-induced transition of the bcc structure to the less permeable fcc structure. The vertical dotted lines in Fig. 4 represent the bcc to fcc phase transition based on the binary phase diagram disregarding any influence of dissolved hydrogen. The small space between the lines represents the mixed phase region. The membrane exhibited fcc permeance values as it was heated to higher temperatures of 1038 and 1173 K and then cooled to 1008 K. On cooling to 623 K, the permeance increased slightly but did not attain the higher bcc permeance level. The membrane was heated again to 738 K with only a small permeance increase and finally to 908 K which resulted in a permeance decrease again corresponding to the fcc level. Based on the observed flux response, the membrane retained the fcc structure, at least partially, when cooled to 623 K. Even after approximately 110 h of flux testing at 623 K, the alloy showed no evidence of attaining the original bcc permeance. No evidence was observed in the permeation behavior at 738 K that suggested a complete phase transformation to bcc. Further discussion of this flux behavior will follow.

Table 2
Phase composition of Pd–Cu alloy membranes

Composition (Pd:Cu, wt.%)	Preparation method	Membrane phase[a] (determined by XRD)	Expected phase (from Fig. 1)
80:20	As brazed[b]	fcc	fcc
60:40	As brazed	fcc	bcc
	Annealed, 588 K, 66 h, in nitrogen	bcc	bcc
60:40 Second preparation	As brazed	Mixed fcc–bcc	bcc
53:47	As brazed	bcc	bcc
40:60	As brazed	fcc	fcc

[a] Alloy phase composition determined at ambient temperature and represents phase present when membrane was loaded into reactor.
[b] Brazed at 1400 K, 4 min, then cooled to ambient over about 5 min.

Two tests were conducted with the 60 wt.% Pd alloy. The initial test (Fig. 5, open circles) was carried out using large temperature steps to assess the alloy's permeance behavior relative to that predicted based on the phase diagram. The permeance of the 60 wt.% Pd alloy measured at 623 K was high but still only about half that of palladium. The permeance diminished when temperature increased above about 840 K (the approximate temperature at which the bcc to fcc transition occurs as shown in Fig. 1) to 908 K. The membrane was then heated to 1038 and 1173 K. The permeance values at 908, 1038 and 1173 K were well correlated by an Arrhenius-type equation and corresponded to fcc phase permeance values that were about one-tenth that of pure palladium. The membrane was then cooled to 623 K (triangle A). At 623 K, the permeance was low but slightly above the level predicted from the fcc Arrhenius correlation. The observed permeance at 623 K also was not stable but was very slowly increasing with time. This permeance increase probably reflected a slow phase transition from fcc back to the more permeable bcc. The membrane was then heated to 738 K (triangle B) and maintained at this temperature for 74 h in an attempt to accelerate the transition to bcc. The membrane was then cooled back to 623 K (triangle C) and maintained at this temperature for an additional 22 h. The permeance had increased but remained less than that of the initial 623 K bcc permeance. Again, the permeance was not stable but very slowly increasing with time indicating continuing phase transition to bcc.

The second 60 wt.% Pd alloy was heated from 623 K through the phase transition to 898 K in 25 K increments allowing the permeance to reach equilibrium at each condition. For this test, the hydrogen partial pressure was held constant at 0.47 MPa. Once the phase transition was complete, larger temperature steps were taken to a final temperature of 1173 K. These results are shown in Fig. 5 (solid diamonds) with permeance results of the first 60 wt.% Pd alloy. At the initial temperature of 623 K, the permeances of the two membranes matched well. In the first stage, as the temperature increased up to 750 K, the permeance increased. In the second stage, from 750 to 875 K, the permeance decreased and, in the third stage, from 875 to 1173 K, the permeance again increased. The permeance increase above 875 K also matched the permeance of the previous 60 wt.% Pd alloy well. These permeance behavior stages can be explained by comparing the results to the phase diagram. The temperature of the first stage corresponds to a phase composition of all or mostly bcc structure which would have a high permeance. The permeance increase relative to temperature increase during this stage is slightly lower than might be predicted based on comparison to palladium or 80 wt.% Pd (fcc throughout the studied temperature range of 623–1173 K) (Fig. 6) or to 53 wt.% Pd (all bcc below about 873 K and all fcc above this temperature). This lower effect of temperature on permeance is probably due to an increase in the proportion of fcc to bcc as the temperature is increased, i.e., the phase composition moves more into the mixed phase region. The second stage, decreasing permeance with increasing temperature, corresponds to the temperature range where the composition diverges more sharply into the mixed phase region. The proportion of fcc increases more quickly as temperature increases until the alloy converts completely to fcc at about 875 K. The third stage reflects a well-behaved Arrhenius-type correlation of permeance increase with temperature increase.

Two other alloy compositions were tested; 40 and 80 wt.% Pd. These compositions were selected to bracket the bcc/mixed bcc–fcc region of the phase diagram.

The phase diagram (Fig. 1) indicates that the 80 wt.% Pd alloy should have an fcc structure over the entire temperature range examined. When tested, this alloy exhibited permeance values of roughly 30% of pure palladium over the 623–1173 K temperature range, as shown in Fig. 6. Although the 80 wt.% Pd alloy was less permeable than the 60 wt.% Pd alloy at 623 K, an Arrhenius correlation fit all of the permeance values (except 1173 K as will be discussed further). The 80 wt.% Pd alloy exhibited higher permeance values than the 53 wt.% Pd alloy at all temperatures, while it exceeded the permeance of the 60 wt.% Pd alloy at temperatures greater than 840 K.

The 40 wt.% Pd alloy is expected to be completely fcc above about 698 K. Below this temperature, the phase diagram [17] suggests a more complex phase behavior. This phase region is not expected to impact the test results for this composition since the flux below 698 K was not detectable. The permeance between 738 and 1173 K (Fig. 6) was very low, about one thousandth that of palladium. An Arrhenius correlation also fit all of the permeance values for this alloy (except 1173 K as will be discussed further).

All of the membranes examined in this study exhibited some decline in permeance when held at 1173 K for an extended period of time. This decline was most pronounced for the 80 wt.% Pd alloy (Fig. 7) which showed a permeance decline of about 0.5% h^{-1} at 1173 K. As the temperature

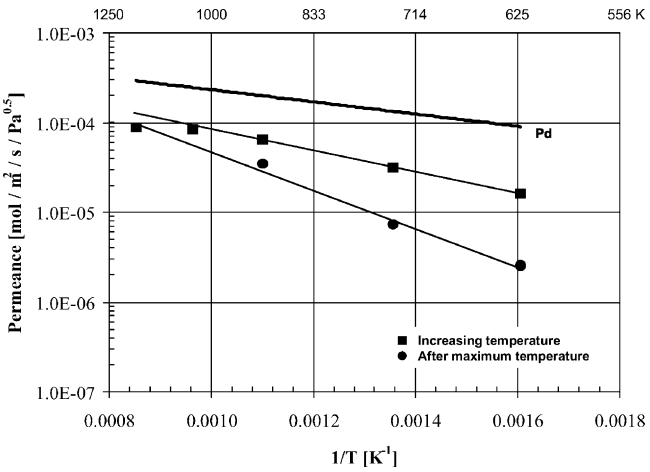

Fig. 7. Permeance of the 80 wt.% Pd alloy as a function of inverse temperature showing the permeance loss attributed to intermetallic diffusion.

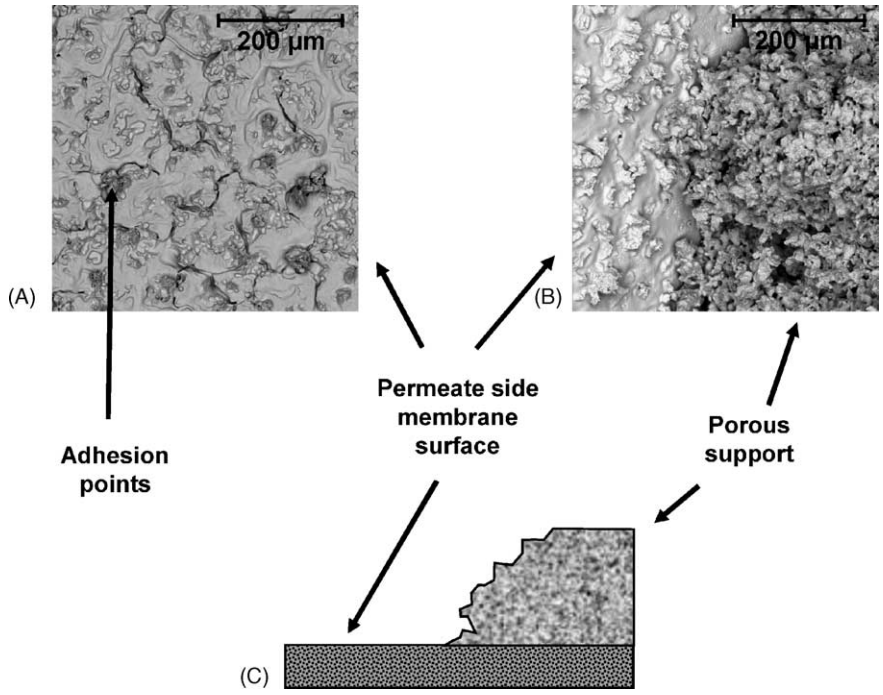

Fig. 8. SEM images illustrating adhesion points and damage to the membrane surface. Image (A) is the surface contacting the porous support for the 80 wt.% Pd alloy. Image (B) shows the surface contacting the porous support for the 60 wt.% Pd alloy with part of the porous support still attached. The schematic (C) shows the idealized cross section of the sample shown in (B).

of this membrane dropped, the permeance remained below the permeance measured during the increasing temperature portion of testing. This membrane was separated from the support for examination after flux testing. During the separation procedure, it was noted that the membrane foil had adhered to the porous support. This adhesion was also noted when the 40, 53, 60 wt.% Pd membranes were disassembled. SEM/EDS analysis showed that the membrane foils had fused to the porous support as indicated by distorted areas where the foils and support had been ripped apart. Examples of this adhesion for the 60 and 80 wt.% Pd alloys are shown in Fig. 8. EDS of these contact points showed that Hastelloy fragments remained attached to the foil. In addition, EDS analysis of membrane foil areas away from these contact points provided evidence of significant intermetallic diffusion as shown in Fig. 9. Ni, Cr and Fe, major components of Hastelloy, were detected in all areas examined on the permeate side of the membrane. This membrane–support interaction was observed in all membranes examined following testing at 1173 K and may be responsible for the observed permeance decline at 1173 K. This permeance decline is possibly due to crystal structure effects from the intermetallic diffusion. Intermetallic diffusion could also be responsible for the failure of the 53 and 60 wt.% Pd alloy

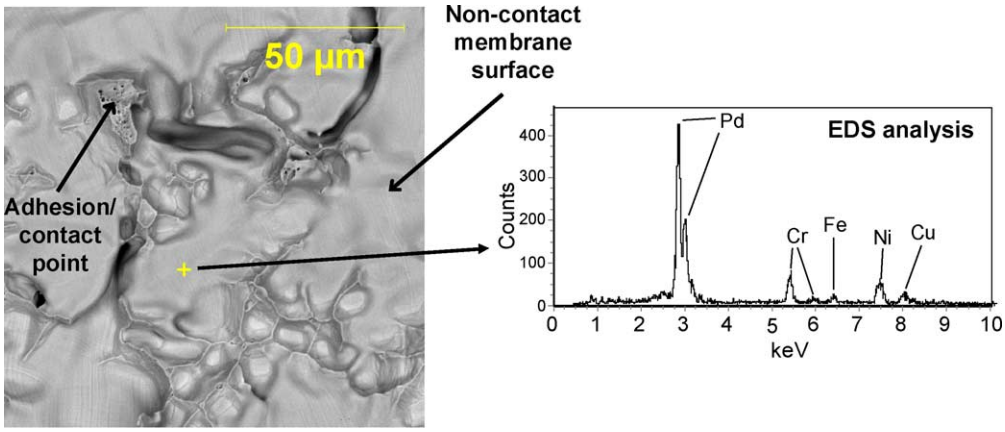

Fig. 9. SEM and EDS images illustrating typical diffusion of Ni, Fe and Cr into membrane foil. Sample shown is the 80 wt.% Pd alloy.

to convert to the bcc structure on cooling into the bcc stable region during testing as noted earlier, although further experimentation is necessary for verification.

It is well known that diffusion barriers or passivation layers can be used to prevent or reduce intermetallic diffusion [12,24]. To investigate the effectiveness of a diffusion barrier, especially at the extreme temperatures of this study, and simultaneously, to verify that the intermetallic diffusion detected by EDS was responsible for the permeance losses observed at 1173 K and on cooling from 1173 K, a diffusion barrier was employed in the second test of the 53 wt.% Pd alloy. The diffusion barrier used for this test consisted of a porous alumina sheet sandwiched between the membrane foil and the porous support but not bonded to either structure.

For the repeat test of the 53 wt.% Pd alloy, small temperature steps were taken through the phase transition to verify that the transition occurred sharply as indicated by the initial permeance test and, also, the phase diagram. Hydrogen partial pressure was again held constant at 0.47 MPa. Once the maximum temperature of 1173 K was attained, the temperature was stepped down to examine the effectiveness of the diffusion barrier. The membrane was held at each temperature until the flux reached a constant value. The results of this test are shown in Fig. 10 along with the initial non-passivated test results. A vertical line indicates the expected phase transition temperature for the binary Pd–Cu alloy at this composition. The temperature increase permeances, indicated by solid diamonds, reproduced the first measured permeances showing that the diffusion barrier did not affect the permeance measurement. The flux up to 873 K reflected the higher permeance associated with the bcc structure. At 885 K, the permeance dropped sharply reflecting the (nearly complete) conversion to the fcc structure. At 898 K, the transition was complete. From 898 to 1173 K, the lower permeance of the fcc structure was observed. The membrane temperature was then reduced to selected values (1038 and 923 K, fcc structure and 848, 723 and 623 K, bcc structure) indicated by open diamonds. For this test, the permeance values measured during cool down matched those measured while increasing temperature indicating no degradation in membrane performance after 72 h at or above 1038 K. These results demonstrate that a diffusion barrier functions well for these membranes.

To examine the effect of the barrier layer on the interface between the membrane surface and porous support, the 53 wt.% Pd alloy membrane utilizing the barrier layer was removed from the reactor and cut apart for characterization following completion of the test series. During disassembly, it was noted that the barrier layer had prevented the membrane foil from fusing to the porous support. The membrane surface contacting the barrier layer was analyzed by SEM/EDS (Fig. 11). Contact points between the aluminum oxide barrier layer and the membrane surface were easily detected (Fig. 11A) as well as surface morphological changes (Fig. 11A and B). EDS analysis of contact points (for example, Fig. 11C) as well as away from these points indicated no detectable intermetallic diffusion. Traces of the aluminum oxide barrier were detectable. The barrier layer cracked during the test cycle or during assembly as expected for this type of layer. The resulting cracks in the barrier layer were reflected in the morphology of the membrane surface (Fig. 11B).

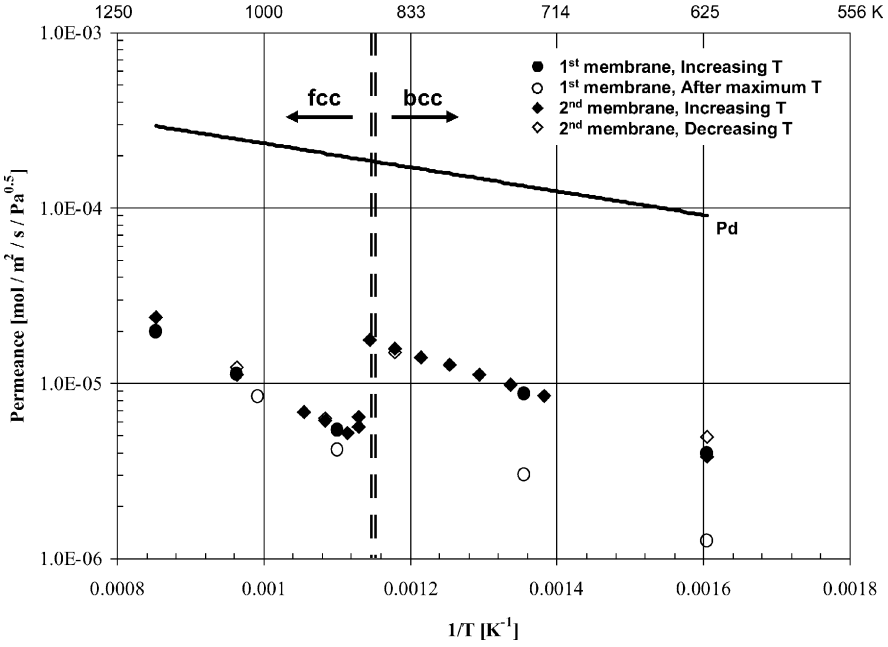

Fig. 10. Permeance of the 53 wt.% Pd alloy as a function of inverse temperature without and with the diffusion barrier between the porous support and membrane.

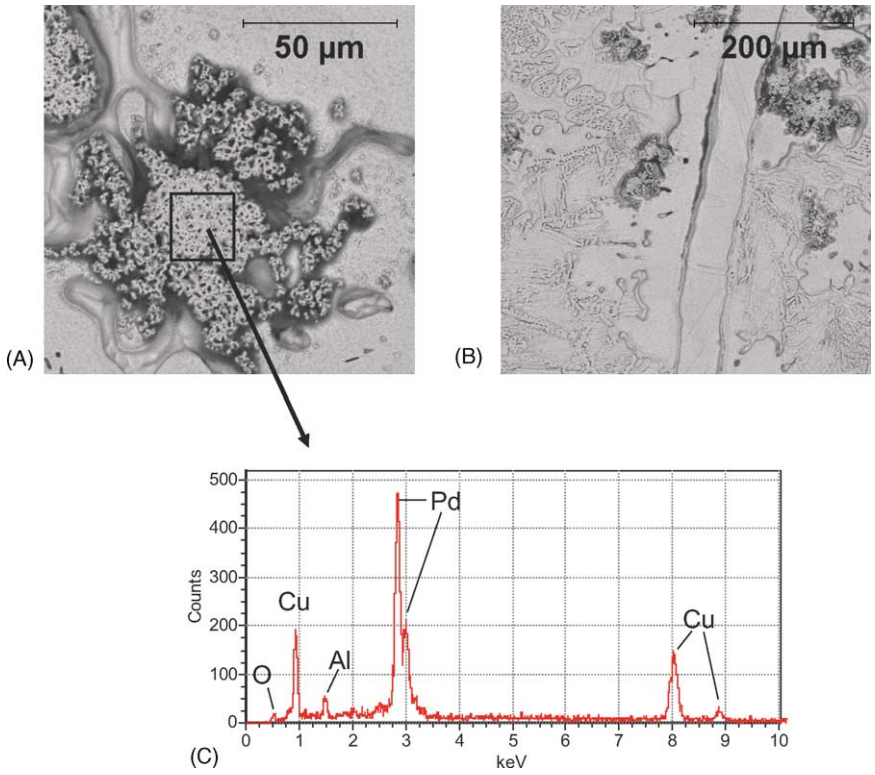

Fig. 11. SEM images showing contact points between the aluminum oxide barrier layer and the permeate side membrane surface (A) and surface morphological changes (A and B). Vertical "channel" in (B) is the imprint of a barrier layer crack. (C) is an example of a typical EDS analysis of a contact point showing no detectable evidence of intermetallic diffusion.

4. Conclusions

The Pd–Cu alloys examined in this study exhibit hydrogen permeance values intermediate to palladium and copper over the 623–1173 K temperature range and 0.1–2.6 MPa pressure range. The 53 and 60 wt.% Pd alloys exhibited relatively high permeance values at temperatures corresponding to bcc crystal structure. Although the 53 wt.% Pd alloy exhibited bcc permeance values over a wider range of temperature, up to 873 K, the 60 wt.% Pd alloy exhibited the highest permeance value (relative to pure palladium) after equilibration at 623 K. The permeance of the 60 wt.% Pd alloy dropped markedly at temperatures greater than 748 K due to the transition of the Pd–Cu crystal structure from bcc or mixed bcc–fcc to fcc. Although the permeance of the 80 wt.% Pd alloy was less than that of the 60 wt.% Pd alloy at 623 K, the 80 wt.% Pd alloy exhibited greater permeance values at temperatures greater than or equal to 738 K. All Pd–Cu alloys are fcc in structure from about 873 K up to their melting point. Within this range, the permeances of the alloys in this study increased steadily with their proportion of palladium, approaching the permeance of pure palladium.

At 1173 K, a slow decline in permeance was noted for all Pd–Cu alloy membranes. This decline was attributed to intermetallic diffusion between the membrane and the support. The failure of the 60 wt.% Pd and the 53 wt.% Pd alloys to attain the high bcc permeance values observed during their initial temperature increase, even after relatively long times with the temperature held within the bcc stability field, was also attributed to intermetallic diffusion effects. An aluminum oxide diffusion barrier was employed to prevent intermetallic diffusion between the porous support and the membrane foil. The barrier layer successfully blocked intermetallic diffusion without degrading permeance performance as shown by the results of the second 53 wt.% Pd membrane test and by SEM/EDS analysis of the membrane following testing. With the application of the barrier, permeance values measured during the temperature increase from 623 K to 1173 K matched the values measured during the temperature decrease back to 623 K. Future work will be directed at determining the temperature and composition range (and corresponding crystal structure) over which various Pd–Cu alloys exhibit resistance to sulfur poisoning as well as the surface chemistry of poisoning resistance.

Acknowledgements

The Hydrogen Membrane Testing Unit at NETL used in this study was operated and maintained by R.P. Hirsh, P.E. Dieter and M.A. Ditillo of Parsons Federal Services Inc. Reference in this paper to any specific commercial product, process, or service is to facilitate understanding and does

not necessarily imply its endorsement or favoring by the US Department of Energy.

References

[1] U. Feuerriegel, W. Klose, S. Sloboshanin, H. Goebel, J. Schaefer, Deactivation of a palladium-supported alumina catalyst by hydrogen sulfide during the oxidation of methane, Langmuir 10 (1994) 3567.

[2] D. Edlund, D. Friesen, B. Johnson, W. Pledger, Hydrogen-permeable metal membranes for high-temperature gas separations, Gas Purif. Sep. 8 (1994) 131.

[3] P. Gravil, H. Toulhoat, Hydrogen, sulphur and chlorine coadsorption on Pd(1 1 1): a theoretical study of poisoning and promotion, Surf. Sci. 430 (1999) 176.

[4] M. Kajiwara, S. Uemiya, T. Kojima, Stability and hydrogen permeation behavior of supported platinum membranes in presence of hydrogen sulfide, Int. J. Hydrogen Energy 24 (1999) 839.

[5] D.L. McKinley, Metal alloy for hydrogen separation and purification, US Patent 3,350,845 (1967).

[6] D.J. Edlund, A membrane reactor for H_2S decomposition, DOE/ER/81419-97/C0749, Contract DE-FG03-92ER81419.

[7] D.L. McKinley, Method for hydrogen separation and purification, US Patent 3,439,474 (1969).

[8] G.J. Grashoff, C.E. Pilkington, C.W. Corti, The purification of hydrogen — a review of the technology emphasizing the current status of palladium membrane diffusion, Platinum Met. Rev. 27 (1983) 157.

[9] A.G. Knapton, Platinum Met. Rev. 21 (1977) 44.

[10] S. Uemiya, N. Sato, H. Ando, Y. Kude, T. Matsuda, E. Kikuchi, J. Membr. Sci. 56 (1991) 303.

[11] W. Juda, C.W. Krueger, R.T. Bombard, Method of producing thin palladium–copper and the like, palladium alloy membranes by solid–solid metallic interdiffusion, and improved membrane, US Patent 6,238,465, 2001.

[12] S.-E. Nam, K.-H. Lee, Hydrogen separation by Pd alloy composite membranes: introduction of diffusion barrier, J. Membr. Sci. 192 (2001) 177.

[13] D.J. Edlund, A catalytic membrane reactor for facilitating the water-gas-shift reaction at high temperatures, phase II, Final Report to the US DOE on Grant DE-FG03-91ER81229 Bend Research, 1995.

[14] B.D. Morreale, M.V. Ciocco, R.M. Enick, B.I. Morsi, B.H. Howard, A.V. Cugini, K.S. Rothenberger, The permeability of hydrogen in bulk palladium at elevated temperatures and pressures, J. Membr. Sci. 212 (2003) 87.

[15] J. Piper, Diffusion of hydrogen in copper–palladium alloys, J. Appl. Phys. 37 (1966) 715.

[16] A.S. Zetkin, G.E. Kagin, A.N. Varaksin, E.S. Levin, Diffusion and penetrability of deuterium in the alloy Pd–53 at.% Cu, Sov. Phys. Solid State 34 (1992) 83.

[17] M.E. Drifts, N.R. Bochvar, L.S. Guzei, E.V. Lysova, E.N. Nadezhnova, L.L. Rokhlin, N.A. Turkina, Binary and Multicomponent Copper-Based Systems, Nauka, Moscow, 1979.

[18] P.R. Subramanian, D.E. Laughlin, Cu–Pd (copper–palladium), in: T.B. Massalski (Ed.), Binary Alloy Phase Diagrams, second ed., ASM International, 1990, pp. 1454–1456.

[19] M. Henson, Constitution of Binary Alloys, McGraw-Hill, 1958, pp. 612–613.

[20] F. Roa, M.J. Block, J.D. Way, The influence of alloy composition on the H_2 flux of composite Pd–Cu membranes, Desalination 147 (2002) 411.

[21] F. Roa, J.D. Way, R.L. McCormick, S.N. Paglieri, Preparation and characterization of Pd–Cu composite membranes for hydrogen separation, Chem. Eng. J. 93 (1) (2003) 11.

[22] Y.H. Ma, I.P. Mardilovich, E.E. Engwall, Thin composite palladium and palladium/alloy membranes for hydrogen separations, Ann. N. Y. Acad. Sci. 984 (2003) 346.

[23] K.S. Rothenberger, B.H. Howard, R.P. Killmeyer, A.V. Cugini, R.M. Enick, F. Bustamante, M.V. Ciocco, B.D. Morreale, R.E. Buxbaum, Evaluation of tantalum-based materials for hydrogen separation at elevated temperatures and pressures, J. Membr. Sci. 218 (2003) 19.

[24] D.J. Edlund, J. McCarthy, The relationship between intermetallic diffusion and flux decline in composite-metal membranes: implications for achieving long membrane lifetime, J. Membr. Sci. 107 (1995) 147.